Lattice model for hydrogen bonding and hydration in pure lipid bilayers

Zhengping Zhang, Jan Tobochnik,* and Martin J. Zuckermann
Centre for the Physics of Materials, Department of Physics, McGill University, Rutherford Building, 3600 University Street, Montréal, Québec, Canada H3A 2T8

John Silvius
Department of Biochemistry, McGill University, Montréal, Québec, Canada H3A 2T8
(Received 13 August 1992)

We propose a model for phase transitions involving hydrogen bonding in lipid bilayers. The model is an interacting model with five states on each site of a two-dimensional square lattice. This model describes both the hydrogen bonding network proposed for phosphatidylethanolamine lipids by x-ray spectroscopy and its disruption by lipid-water interactions. The phase transitions predicted by the model are identified by use of numerical simulation in conjunction with recent extrapolation and finite-size-scaling methods. The percolation properties were also investigated, and it is found that the percolation exponents cannot be described by random percolation theory. The relationship of the results to experiment and extensions of the model is discussed.

PACS number(s): 87.22.Bt, 64.60.Cn, 64.60.Ak

I. INTRODUCTION

Both anhydrous and fully hydrated phospholipid bilayers have been the subject of much experimental and theoretical work due to their interesting phase behavior. In addition, hydrated bilayers are considered to be models for biological membranes. Generally phospholipids are surfactantlike molecules with two hydrophobic fatty acid chains and a hydrophilic polar head. The nature of the polar head is therefore important for the hydration properties of the bilayer. Two types of polar head, phosphorylcholine (PC) and phosphorylethanolamine (PE), together account for the polar heads of the majority of phospholipids in most cell membranes [1]. Lamellar phases composed of PE hydrate less strongly than the corresponding lamellar phases of PC [2], and show a much greater tendency to form dehydrated and/or nonlamellar phases than do PC lipids of comparable acyl chain composition.

Boggs [3] and Hauser *et al.* [4] have suggested that the differences in the hydration properties of PE and PC lipids are largely attributable to differences in the abilities of these two lipids to participate in intermolecular lipid-lipid hydrogen bonding. The hydrogen bonding of dilauroylphosphatidylethanolamine (DLPC) has been investigated by using x-ray crystallography by Hitchcock *et al.* [5], who found that in anhydrous crystals each PE polar head was connected by N–H$\cdots$O hydrogen bonds to four neighboring polar heads. Here the the bonds are between the oxygens (acceptors) of the phosphate group and the hydrogens (donors) of the amino group. Since the trimethylammonio group of PC lipids cannot form hydrogen bonds, the PC headgroup can serve as an acceptor but not as a donor of hydrogen bonds.

Fully hydrated one-component PC bilayers undergo a phase transition, known as the main phase transition, in which the bilayer passes from a gel (solid) phase to a liquid–crystalline (fluid) phase. Both these phases are stable hydrated phases. For pure PE lipid bilayers, the situation is considerably different. Several studies [6–11] have shown that aqueous dispersions of dimyristoyl phosphatidylethanolamine (DMPE) can form at least three distinct types of lamellar phase: stable, virtually dehydrated "crystalline" (AS) phases in which the acyl chains are rigid and tightly packed and the polar heads are presumably hydrogen bonded to one another; a hydrated solid (HS) metastable phase, in which the chains are somewhat less tightly ordered; and a hydrated fluid (HF) stable phase, in which the chains are flexible. The crystalline nature of the AS phase has been confirmed by the x-ray crystallographic studies of Seddon and coworkers [6, 7], who show that this phase has basically the same structure as the anhydrous crystal. On heating, the AS phase makes a first-order phase transition to the HF phase. Several effects occur at this transition. Firstly, the solid melts and the acyl chains become flexible (chain melting). A second likely effect in the HS and HF phases is that the interlipid hydrogen bond network existing in the AS phase could be disrupted by competition with lipid-water interactions. The precise degree to which interlipid hydrogen bonding interactions are disrupted upon conversion of the AS phase to the HS or HF phase has yet to be established experimentally, although it appears that lipid-water hydrogen bonding is extensive in the HF phase in particular. In contrast to the AS to HF transition, the transition of the metastable, but long-lived HS phase to the HF phase exhibits a considerably lower latent heat. One implication is that the hydrogen bonding makes almost no contribution to the latent heat of the transition between the hydrated phases.

There have been a number of models relevant to hydrogen bonding in lipid bilayers. The earlier models were

phenomenological models for the effect of hydrogen bonding on the transition temperature of the main phase transition proposed by Nagle [12] and Eibl and Wooley [13]. A more recent microscopic model, which is the closest one to the model we propose in this paper, is that studied in considerable detail by MacDonald, Pink, and Quinn [14, 15]. Their model applies to those hydrated ceribrosides in which there is a single-donor–single-acceptor complex on the amide group giving rise to a "striped" ground state composed of one-dimensional (1D) hydrogen bonding networks. This model included both hydrogen bonding effects and chain melting at the main phase transition. This model is similar to a Potts lattice gas model of krypton adsorbed on graphite proposed by Berker, Ostlund, and Putnam [16] and a site-bond percolation model, with temperature-dependent bond probability proposed by Coniglio, Stanley, and Klein [17] to study the sol-gel transition. Both models include a site degree of freedom which cannot bond with neighboring sites, and other degrees of freedom which are able to, but need not, bond with neighboring sites. Also, in both models the bonds are not correlated with the relative position of the sites. This is a major difference between the latter two models, and both the first model and the one we propose in Sec. II.

In the present work we concentrate on the hydrogen bonding aspects of the main phase transition of pure PE bilayers and study the related percolation properties in detail. A detailed analysis of chain melting will be the subject of a later study. In Sec. II, we present an interacting model with five states on each site of a 2D square lattice. This model mimics both the hydrogen bonding network proposed for PE lipids by Hitchcock *et al.* [5, 4] and its disruption by lipid–water interactions. Four of the states describe the bonding aspects of the double-donor–double-acceptor complex of PE polar heads leading to a 2D network of hydrogen bonds and the fifth state is an unbonding state which is related to hydration effects. The parameters of the model are the bonding energy, E_b, and the degeneracy, D_u, of the unbonding state. In our work, a high value of D_u implies that the degeneracy of the fifth state includes the degeneracy of melted lipid chain conformations typical of the HF phase. We study the phase behavior of the model by computer simulation and use the recently proposed finite-size-scaling method of Lee and Kosterlitz [18] to examine the nature of the related phase transitions. Both the methods and the simulation results are described in Sec. III. We find a percolation transition at a temperature T_p, which decreases with increasing degeneracy. The transition is a continuous percolation transition without any thermal phase transition below a critical value of D_u, and above this value there is a first-order thermal transition accompanied by a first-order percolation transition. The low temperature phase which is almost fully bonded represents the AS phase, and the high temperature phase models a hydrated HS or HF phase. A numerical study of the scaling behavior of the percolation transition is presented in Sec. IV. In this section, it is shown that the percolation exponents of our model are more closely related to bootstrap percolation than to regular percolation theory. Section V contains a discussion of the results of Secs. IV and V in the context of experiment and concludes the article.

II. MICROSCOPIC MODEL FOR HYDROGEN BONDING

In this section we give a detailed description of the microscopic model used to describe the hydrogen bonding network of polar heads discussed in Sec. I. The network is set up on a two-dimensional square lattice with a lattice spacing set to unity. Each lattice site represents a PE polar head which can have a maximum of four possible hydrogen bonds (HB's) with the polar heads of neighboring molecules. Each polar head has two HB donors and two HB acceptors. The structure of the polar head is such that the two donors are perpendicular to each other and the donors are antiparallel to the acceptors. This is the case for PE polar heads in DLPC [5]. Each lattice site represents a PE polar head and can be in one of five possible states. Four of these states are called bonding states, and we assume that for the bonding states the donors are oriented along the links between lattice sites. Since the two donors are perpendicular we associate with each bonding state a horizontal unit vector $\mathbf{S}^{(x)}$ corresponding to the direction of one of the donors and a vertical unit vector $\mathbf{S}^{(y)}$ corresponding to the direction of the other donor at the same site. Thus, the four bonding states are given by $(\mathbf{S}^{(x)} = \hat{\mathbf{x}}, \mathbf{S}^{(y)} = \hat{\mathbf{y}})$, $(\mathbf{S}^{(x)} = \hat{\mathbf{x}}, \mathbf{S}^{(y)} = -\hat{\mathbf{y}})$, $(\mathbf{S}^{(x)} = -\hat{\mathbf{x}}, \mathbf{S}^{(y)} = \hat{\mathbf{y}})$, and $(\mathbf{S}^{(x)} = -\hat{\mathbf{x}}, \mathbf{S}^{(y)} = -\hat{\mathbf{y}})$. This allows three possible arrangements on each lattice bond connected by bonding states: two donors, two acceptors, or one donor and one acceptor. In our model, a hydrogen bond of bonding energy, E_b, is formed when an acceptor and a donor are present on the same lattice bond. The two other arrangements have no energy associated with them. The system lowers its energy by an amount E_b when an HB is formed and the same value of the energy is required to break an HB. Note that on each site it is possible for one of the HB donor vectors, $\mathbf{S}^{(x)}$ or $\mathbf{S}^{(y)}$, to bond without the other donor bonding. The same is true for the acceptors. Thus, from zero to four HB's can be formed between a site and its four nearest neighbors. The polar head is also allowed to be in a fifth state, called the "unbonding" state [14, 19]. This state has a degeneracy D_u, which partially represents all possible orientations of the polar head, both in-plane and out-of-plane, for which a polar head cannot form hydrogen bonds with neighboring polar heads. In this work, we assume that the degeneracy is principally a measure of the ability of the polar head to become hydrated by the surrounding water molecules at low values, but includes melted chain conformation at higher values of D_u. The thermally induced competition between the formation of HB's and the degeneracy effect of the unbonding state should therefore result in a hydration-dehydration transition. For the unbonding state the donor vectors are assigned the values $\mathbf{S}^{(x)} = \mathbf{0}$ and $\mathbf{S}^{(y)} = \mathbf{0}$. The five states at each lattice site of the model and some of the various bonding possibilities are shown in Fig. 1.

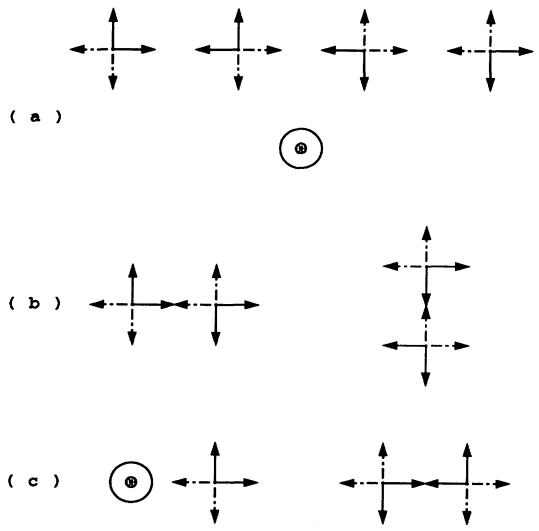

FIG. 1. (a) The five possible states at each lattice site of our model. The solid vectors point in the direction of the HB donors and are equal to $\mathbf{S}^{(x)}$ and $\mathbf{S}^{(y)}$. The dashed vectors represent the direction of the HB acceptors. The fifth state is schematically represented as a circle with a dot inside, and is shown in the second row. (b) Two of the bonding possibilities for nearest-neighbor sites. (c) Two examples of nearest-neighbor sites which do not bond.

The Hamiltonian for the five-state model described above can be written as follows:

$$\mathcal{H} = -E_b \sum_i [f(\mathbf{S}^{(x)}_{\mathbf{r}_i} \cdot \mathbf{S}^{(x)}_{\mathbf{r}_i+\hat{\mathbf{x}}}) + f(\mathbf{S}^{(y)}_{\mathbf{r}_i} \cdot \mathbf{S}^{(y)}_{\mathbf{r}_i+\hat{\mathbf{y}}})], \quad (1)$$

where $f(1) = 1$, $f(z) = 0$ for $z \neq 1$, and $\mathbf{S}^{(x)}_{\mathbf{r}_i}$ and $\mathbf{S}^{(y)}_{\mathbf{r}_i}$ represent the donor vectors of the ith polar head located at the position $\mathbf{r}_i$. Finally, Mouritsen [20] has shown how degeneracies such as D_u should be treated in Metropolis Monte Carlo simulations. We wish to point out that degeneracies for states representing an average over melted chain conformations can be quite high (see [20]).

III. CALCULATIONAL TECHNIQUES AND PHASE DIAGRAM

We begin this section with a short description of the finite-size-scaling methods used to identify the nature of phase transitions in the microscopic model given by Eq. (1). This will be followed by the numerical simulation results obtained from finite-size scaling for this model.

First-order transitions are usually characterized by discontinuities in the first derivatives of the free energy. This results in a δ-function singularity in the specific heat $C(T)$ at the transition in the thermodynamics limit. In a finite system, however, the transition region is broadened and the peak in $C(T)$ is finite and its height increases with increasing linear lattice size, L. Furthermore, the location of the intensity of the maximum varies in a size-dependent manner. The maxima grow as L^d in d dimensions and the δ-function limit is obtained because the width decreases as L^{-d}. The maximum value of $C(T)$ for a finite lattice is

$$C_L^{\max} = a + bL^d, \quad (2)$$

where a and b are the size-independent parameters determined from the model [21]. A similar scaling form exists for the maximum value of other response functions such as the susceptibility in Ising systems. $C(T)$ is calculated from the following expression:

$$C(T)/k_B = \beta^2(\langle E^2\rangle - \langle E\rangle^2)/L^d, \quad (3)$$

where $\beta = \frac{1}{k_B T}$. The phase behavior of the microscopic model of Eq. (1) is examined by the standard Metropolis Monte Carlo method with nonconserved dynamics [20] in conjunction with the new techniques of Ferrenberg and Swendsen [22] and Lee and Kosterlitz [18, 23] to examine the phase behavior of the model. Each Monte Carlo step consists of randomly choosing a site and attempting to change the state of that site to one of the four other states with a probability given by the Metropolis rule. In computing the difference in energy between the old and a new state we use the Hamiltonian of Eq. (1). The Monte Carlo techniques used here consist of three parts. First, Monte Carlo simulations are performed for the evaluation of the specific heat, $C(T)$ as a function of temperature T, using Eq. (3). The results of these simulations are used to determine the peaks in $C(T)$ as accurately as possible.

Next, long time simulations are performed at the position, T_0, of the peak of $C(T)$ for several values of the system size, L. Here L^d is the volume of the system. The extrapolation method of Ferrenberg and Swendsen is then used to calculate the probability distribution, $P(E, T_0, L)$, of the internal energy at the peak. This method allows one to calculate thermodynamic properties of a system at temperatures near the temperature at which the simulation was actually run. In particular, this allows us to calculate the values of $C(T)$ at neighboring temperatures. Finite-size scaling can then be performed on the data. For a first-order phase transition, $C(T)$ scales according to Eq. (2) whereas it scales as $L^{\frac{\alpha}{\nu}}$ for a continuous transition, α and ν being the usual critical exponents.

The order of the phase transition is then examined by the method of Lee and Kosterlitz. This method consists of calculating the free energy as a function of the internal energy at the transition from the probability distribution at the specific heat peak. The quantity $\mathcal{A}(E, T, L)$ defined by [23]

$$\mathcal{A}(E, T, L) \sim -\ln \mathcal{P}(E, T, L) \quad (4)$$

differs from the bulk free energy $\mathcal{F}(E, L)$ by a temperature- and L-dependent additive quantity. However, at fixed T and L, the shape of $\mathcal{A}(E, T, L)$ will be identical to that of $\mathcal{F}(E, L)$ and also $\Delta\mathcal{A} \equiv \mathcal{A}(E) - \mathcal{A}(E') = \mathcal{F}(E) - \mathcal{F}(E')$. A measurement of $\Delta\mathcal{A}$ therefore gives a direct evaluation of the corresponding $\Delta\mathcal{F}$. At a first-order transition, $\mathcal{F}(E, L)$ has pronounced double minima corresponding to two coexisting phases at $E = E_{1,2}$ separated by a maximum at E_m corresponding to a domain wall between the two phases. The maximum

difference in $\mathcal{F}(L)$ is

$$\Delta\mathcal{F}(L) = \mathcal{F}(E_m, L) - \mathcal{F}(E_1, L) \sim L^{d-1}, \quad (5)$$

and therefore, at a first-order transition, $\Delta\mathcal{F}(L)$ increases monotonically with increasing L. Furthermore, $\Delta\mathcal{F}(L)$ decreases with increasing L in the absence of a transition leading to a single minimum in the thermodynamic limit. Finally $\Delta\mathcal{F}(L)$ is independent of L at a critical point.

The two model parameters are $T^* = k_B T/E_b$ and the unbonding degeneracy, D_u. The finite-size-scaling methods described above were used to obtain a phase diagram in terms of T^* and D_u. We therefore examined the model of Eq. (1) by performing numerical simulations on $L \times L$ square lattices with periodic boundary conditions. The temperature at which the simulations were performed was chosen as close as possible to the transition temperature, T_p^*, and 4×10^6 Monte Carlo steps per site (MCS) were found to give the required accuracy.

The thermal transition at T_p^* found using the model of Eq. (1) is accompanied by a percolation transition. The phase below T_p^* is characterized by an infinite cluster of hydrogen bonds whereas there are only finite HB clusters (lattice animals) above T_p^*. If this transition is a first-order phase transition, then $T_p^* \equiv T_p^*(L)$ will be a function of system size and it is defined as the tem-

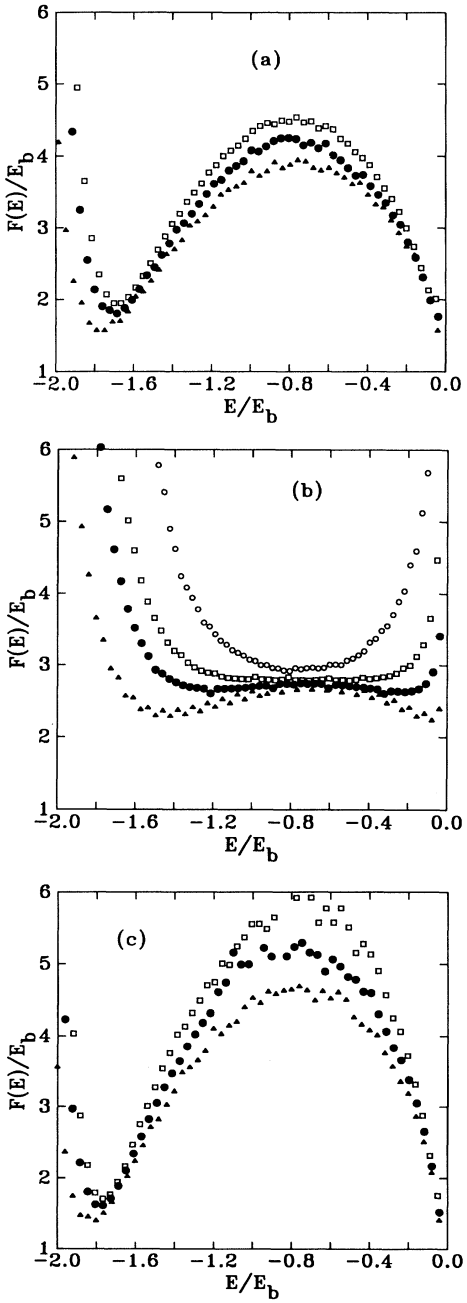

FIG. 2. Free energy $\mathcal{F}(E, L)$ vs E/E_b. D_u = (a) 160, (b) 100, and (c) 200.

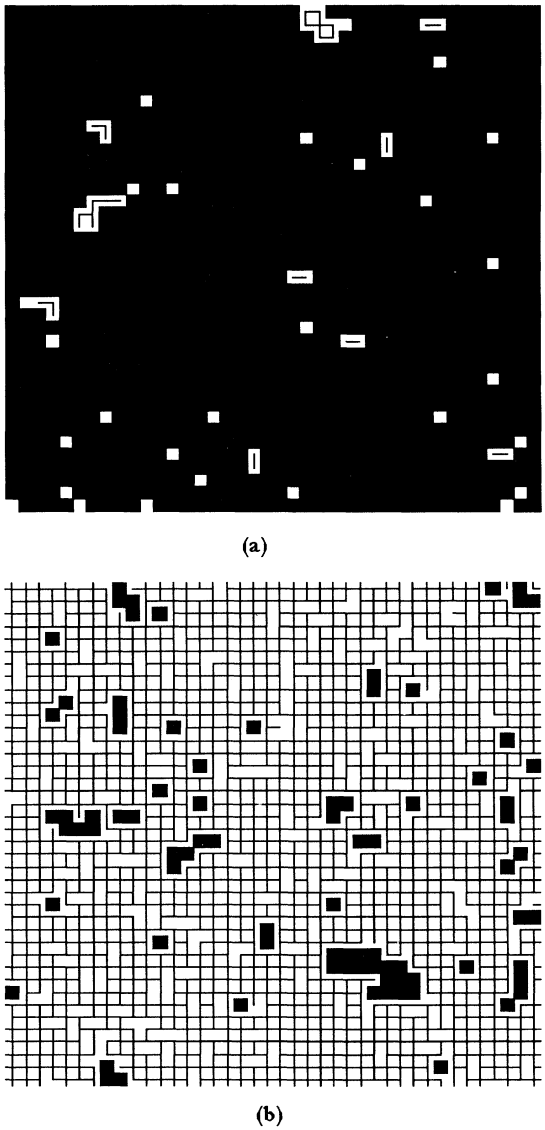

FIG. 3. Configurations for $D_u = 200$. The shaded squares indicate unbonding states. The lines indicate actual HB bonds. (a) $T^* = 1.004T_p^*$. (b) $T^* = 0.996T_p^*$.

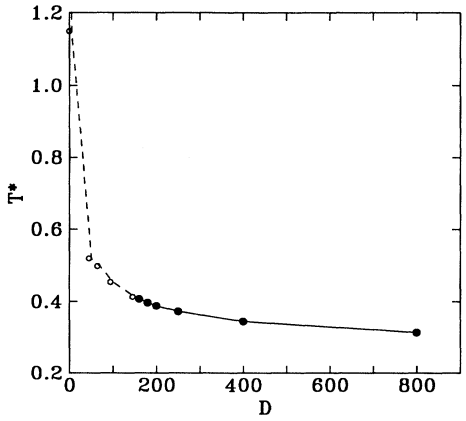

FIG. 4. Phase diagram for our model. The solid line indicates a first-order transition. The dashed line indicates no thermal phase transition, but the existence of a percolation transition.

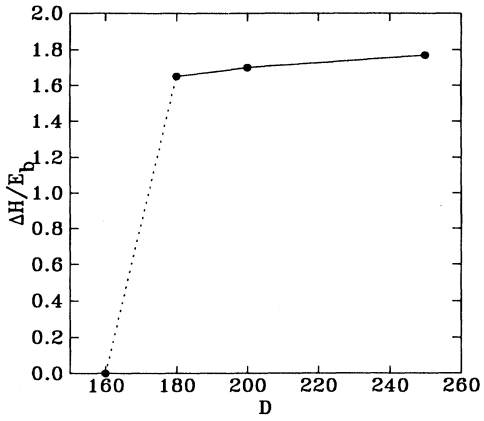

FIG. 6. Latent heat in the regime of first-order phase transitions as a function of D_u. The lines are guides to the eye. The point at $D_u = 160$ is an estimate of the location of the critical point.

perature at which $\mathcal{F}(E_1, L) = \mathcal{F}(E_2, L)$, where $\mathcal{F}(E_1, L)$ and $\mathcal{F}(E_2, L)$ are the free energies of the percolating and nonpercolating phases, respectively. These free energies were calculated for various values of the degeneracy, D_u, from 2 to 800 for L=12, 16, and 20 in order to examine the phase behavior of the system and to find a critical point. It was found that the system did not exhibit a phase transition for values of D_u below about 160. At this value of D_u, the system is at or extremely close to a critical point. Figure 2(a) shows that, in this case, the free energy as a function of E/E_b exhibits two minima with a maximum between them, but that the height of the maximum, $\Delta\mathcal{F}(L)$, is independent of system size to within calculational error. Figure 2(b) gives $\mathcal{F}(E, L)$ as a function of system size and E/E_b when $D_u = 100$. This figure shows that $\Delta\mathcal{F}(L)$ decreases with increasing L in this case implying the absence of a phase transition in the thermodynamic limit. The temperature T_p^* then represents a continuous percolation transition. In contrast, Fig. 2(c) shows that, for $D_u = 200$, $\Delta\mathcal{F}(L)$ increases with increasing L implying the occurrence of a first-order phase transition. In this case the system makes an abrupt transition from the percolating case to a situation where there are only a few clusters of hydrogen bonded polar heads. We also calculated the specific heat at T_p^* for different system sizes when $D_u = 200$ and showed that it increased linearly with increasing $L \times L$. This confirms that the transition is first order [see Eq. (2)]. Bonding configurations just below and just above T_p^* are shown in Fig. 3. The phase diagram for the model is given in Fig. 4, which shows that T_p^* decreases with increasing D_u. Figure 5 shows that the specific heat scales reasonably as a function of system size, L, for $D_u = 200$ with a slight decrease in peak height as L increases. The area under the curve in Fig. 5 gives the latent heat of transition, ΔH, which is shown in Fig. 6 for several values of D_u in the first-order transition regime. The same values for ΔH were found by calculating the difference in free energy between the minima at the respective first-order phase transition (see Fig. 2). Figure 6 shows that the values found for ΔH are of the order of the bonding energy, E_b.

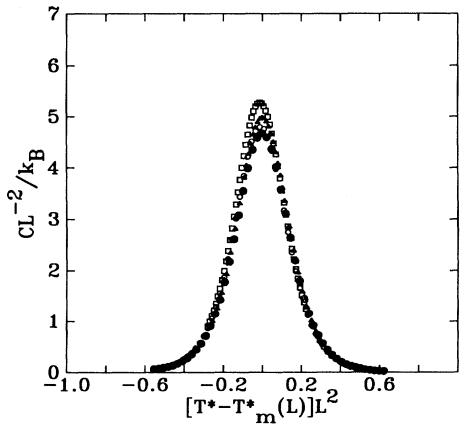

FIG. 5. Scaling function for the specific heat for $L = 12, 16, 20$, and 24, and $D_u = 200$. T_m^* is the location of the specific heat maximum. The peak height of the scaling function decreases with increasing L.

IV. PERCOLATION EFFECTS AT LOW DEGENERACIES

We showed in Sec. III that for D_u less than approximately 160 there is no thermal phase transition in our model. However, there is a percolation transition which occurs when an infinite cluster of sites connected by hydrogen bonds spans the lattice at a definite transition temperature T_p^*. We now wish to determine the critical properties of this transition.

Our system is a natural example of correlated site-bond percolation. A site is occupied if it is in any one of the four bondable states. Two neighboring occupied

sites are connected by a bond only if they have a hydrogen bond according to our model. Most other examples of site-bond percolation in thermally driven systems impose bonds on the system. For example [19], the critical point of the Ising model becomes a percolation transition if one assigns bonds between spins pointing in the same direction with a probability $1-\exp(-2J\beta)$, where J is the Ising nearest-neighbor coupling. The critical percolation exponents in this case are given by their Ising model equivalents. Another example is a model of gelation in microemulsions devised by Stauffer and Eicke [24] which uses a Widom model to investigate three transitions: phase separation when the the magnetization becomes nonzero, electrical percolation when an infinite cluster of up spins is formed, and gelation when an infinite cluster of up spins connected randomly by bonds with probability p_b is formed. Again the bonds are imposed and are not part of the Hamiltonian. When bonds are imposed at random with a particular probability one expects the critical exponents to be the same as those for ordinary percolation. In two dimensions these are given by $\beta = 5/36 \approx 0.14$, $\gamma = 43/18 \approx 2.39$, and $\nu = 4/3 \approx 1.33$ [25]. The exponents are defined by the following power laws near the percolation transition, p_c:

$$P_\infty \sim (p-p_c)^\beta, \tag{6}$$

$$\chi \equiv \sum_s n_s s^2 \sim (p-p_c)^{-\gamma}, \tag{7}$$

$$\xi \sim (p-p_c)^{-\nu}, \tag{8}$$

where P_∞ is the probability of an occupied site belonging to the infinite spanning cluster, n_s is the number of clusters per site with s sites, and ξ is the connectedness length. The sum in Eq. (7) does not include the largest cluster.

To obtain values for the exponents we apply the standard finite-size-scaling relations for a system of size L [25]:

$$P_{\rm span}(L,t) = f(tL^{1/\nu}), \tag{9}$$

$$P_\infty(L,t) = L^{-\beta/\nu} g(tL^{1/\nu}), \tag{10}$$

$$\chi(L,t) = L^{\gamma/\nu} h(tL^{1/\nu}), \tag{11}$$

where $t = (T^* - T_p^*)/T_p^*$, $P_{\rm span}$ equals the probability of the system containing a spanning cluster in the vertical direction, and the exponents and scaling functions, f, g, and h depend on the degeneracy, D_u. The above scaling forms assume that T^* plays the same role as the percolation probability p in random percolation models. We use the standard cluster labeling techniques to enumerate the clusters and calculate χ, P_∞, and $P_{\rm span}$, The Ferrenberg-Swendsen method of calculating properties at temperatures other than the one being simulated also works very well for cluster properties. Using Eq. (9), the temperature T_p^* is determined by the crossing of the curves for $P_{\rm span}$ versus temperature for different sizes. Then the exponents β/ν and γ/ν are obtained from log-log plots using Eqs. (10) and (11), respectively. The exponent ν is obtained from

$$T_p^*(0.8) - T_p^*(0.2) \sim L^{-1/\nu}, \tag{12}$$

where here $T_p^*(x)$ is the temperature at which a fraction x of the configurations span vertically. Scaling plots for $D_u = 100$ and $D_u = 5$ are shown in Figs. 7 and 8.

Our results for $D_u = 100$ are $\nu = 1.28 \pm 0.03$, $\gamma = 2.87 \pm 0.11$, and $\beta = 0.28 \pm 0.04$. The error estimates are based on how the slopes in the log-log plots vary as we vary the estimate of T_p^*. The exponents do not follow the hyperscaling relation $d\nu = \gamma + 2\beta$. The value for ν is reasonably close to that of ordinary random percolation (RP), but the other two exponents are significantly higher. This is similar to the situation in bootstrap percolation (BP) [26, 27]. In m state BP configurations are generated with site probability p, and then occupied sites with fewer than m neighbors are recursively eliminated. This culling tends to increase the value of the percolation threshold for $m > 1$. The case $m = 0$ is ordinary percolation. One expects for $m = 1$ to have the same scaling behavior as RP. For $m = 2$ on a square lattice simulations show that ν is the same as in RP [28] but β is higher [26]. In addition, one can show that β is at least as large as in RP [29]. Although our results are not sufficiently precise to establish any quantitative connection to BP, they do show the same qualitative behavior. Also, for $m > 2$ on a square lattice BP has a first-order transition at $p_c = 1$ just as our model has a first-order transition for large enough degeneracy.

We expect that as $D_u \to 0$ our results should converge to the random percolation scaling behavior. For $D_u = 0$ it is clear that the transition must be at infinite temperature since the site probability is unity and the bond probability at finite temperatures is always less than or equal to 0.5, which is the percolation transition for random bond percolation on a square lattice. Thus, we expect the $D_u = 0$ version of our model to be equivalent to random bond percolation, and we must obtain the ordinary percolation exponents. For $D_u = 5$ we found that

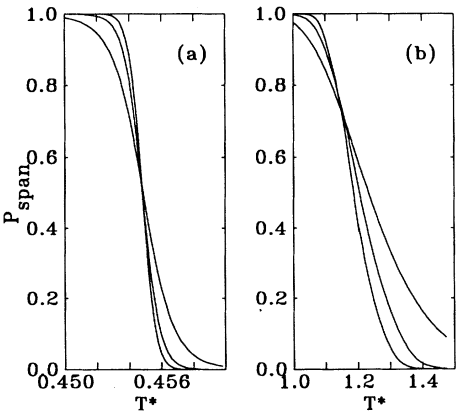

FIG. 7. $P_{\rm span}$ vs T^* for $L = 20, 40$, and 60. The transition region narrows as L increases. (a) $D_u = 100$; (b) $D_u = 5$.

$\nu = 1.39 \pm 0.03$ and $\gamma = 2.72 \pm 0.09$. We are not able to estimate a value for β since the log-log plot of $P_\infty(L)$ shows too much curvature. Note that we include in our scaling plots a point for $L = 8$. For $D_u = 100$ we cannot include such a point because at this size the system behaves as if there is a first-order transition.

We can understand these results quite readily. The effect of the interactions in our model is to fill in the clusters that would be obtained from random percolation. This effect can easily be seen by looking at pictures of configurations as shown in Fig. 9. We see that above the transition there are very few clusters, but very close to the transition there is one large cluster containing almost all the sites. This filling in will not affect the linear extent of the clusters and thus ν will not change. However, since both P_∞ and χ depend on the mass of the clusters, we would expect the exponents describing them to increase, as indeed we have found. Notice also the difference between the configurations at $D_u = 100$ in Fig. 9 and those at $D_u = 200$ in Fig. 3. Even though the configurations we show at $D_u = 200$ is for a smaller $|t|$, the change between just above and just below T_p^* is much greater than those shown for $D_u = 100$. This is what we would expect for a first-order transition.

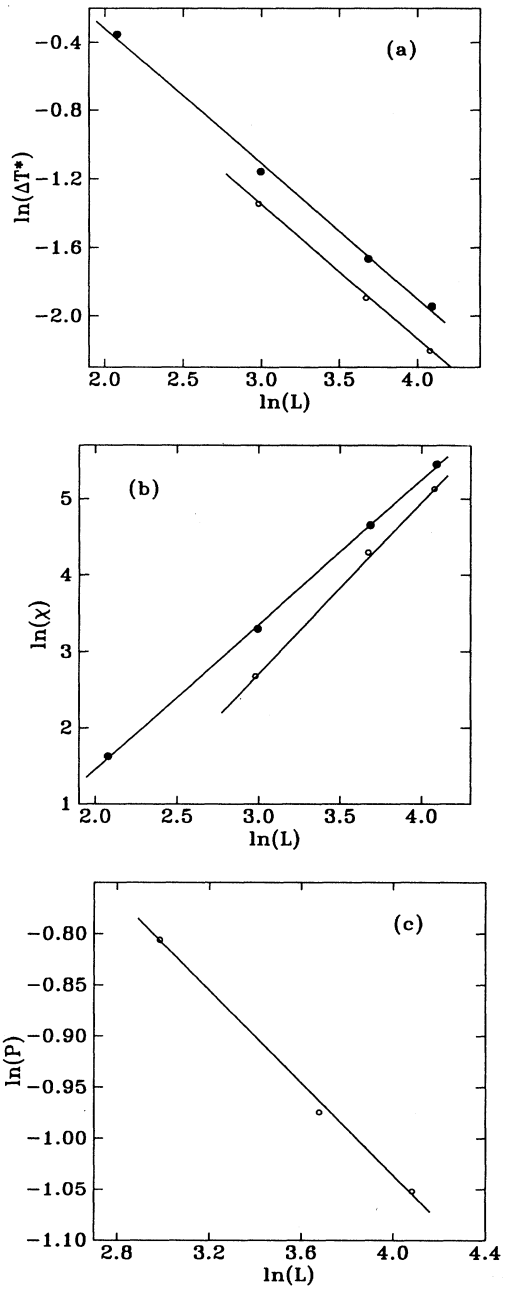

FIG. 8. Scaling plots (a) $\ln \Delta T^* \equiv \ln [T_p^*(0.8) - T_p^*(0.2)]$ vs $\ln L$. (b) $\ln \chi$ vs $\ln L$. For (a) and (b): lower plot for $D_u = 100$; upper plot for $D_u = 5$. (c) $\ln P_\infty$ vs $\ln L$ for $D_u = 100$.

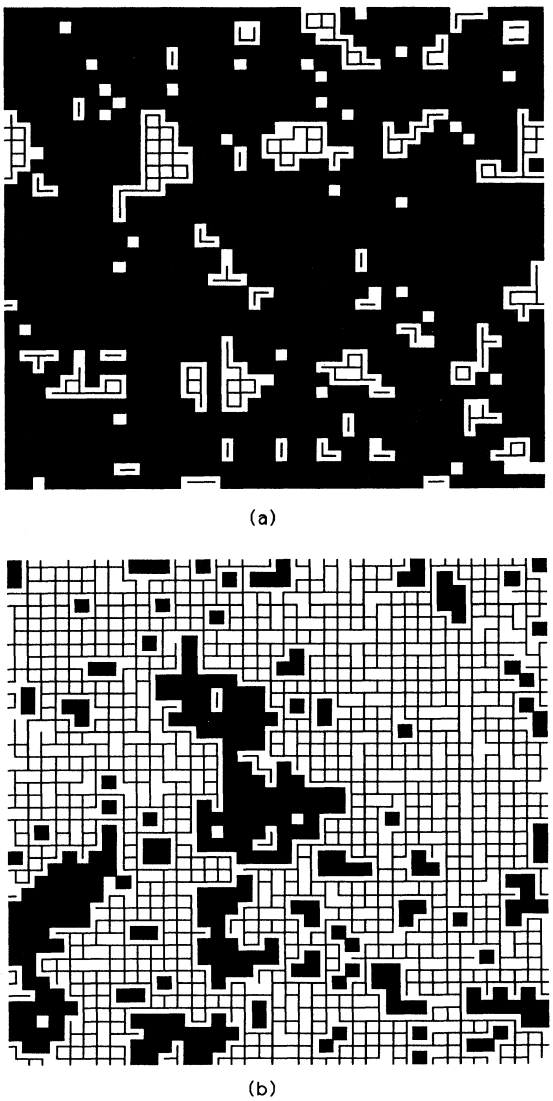

FIG. 9. Configurations for $D_u = 100$. The shaded squares indicate unbonding states. The lines indicate actual HB bonds. (a) $T^* = 1.01 T_p^*$. (b) $T^* = 0.99 T_p^*$.

The presence of a percolation transition without a thermal transition resembles the idea put forward by Adler and Stauffer [30] for a liquid-gas transition line above the critical temperature in the Ising model. They find evidence for a sharp transition line where there is a change in the convergence behavior of the Taylor-series expansion of the magnetization for a system in a large magnetic field. This transition line corresponds to the percolation transition based on the Kertesz droplet definition [31].

The lattice structure of our models should not affect the validity of the above results. In RP the critical exponents are known to depend only on the spatial dimensionality not on the lattice structure. Indeed all static exponents are the same even for continuum percolation models [32]. For BP on a triangular lattice, β is similar for $m = 2$ to the square lattice value [26] and there are first-order transitions for $m > 3$. Thus, we do not expect the scaling behavior of our model to vary much if we change the lattice structure. If we consider our model on a triangular lattice with six possible bonding states, each of which has two HB donors separated by 60°, then there is a maximum of four possible bonds with the six nearest neighbors. Thus, only $2/3 \approx 0.67$ of all possible bonds can be occupied, compared to the square lattice where all bonds can be occupied. However, the bond percolation threshold for the triangular lattice is at about 0.347 [25], which is about 0.69 of the threshold for the square lattice. Since this is roughly the same fraction as the fraction of possible bonds, we would expect that T_p^* as a function of D_u would be similar in the square and triangular lattices.

V. CONCLUSION

In this work we have proposed and analyzed a model for 2D hydrogen bonding networks in lipid bilayers. Our purpose was to understand the phase behavior and percolation properties of these systems in the absence of other more complex effects. We have shown by computer simulation that the model has a percolation transition in the absence of a thermal transition at low values of D_u and a first-order phase transition accompanying the percolation transition for $D_u > 160$. We have investigated in detail the nature of the percolation transition for $0 < D_u < 160$, where there is no thermal transition, and found that the scaling behavior cannot be described by random percolation theory, but is similar to that found in bootstrap percolation. It would be interesting to find a real lipid system which exhibits such a percolation transition without a thermal transition. Such a transition could be inferred from spectroscopic measurements of the number of hydrogen bonds. It would clearly be of more interest to measure the connectivity of the hydrogen bonding network, but this is difficult to achieve with present experimental techniques. However, Lamanna and Cannistraro [33] recently showed that data from proton nuclear magnetic resonance experiments on normal and supercooled water could be interpreted in terms of the cooperativity of the hydrogen bonding network. It would therefore be of interest to see if this experimental method could also be used for the examination of hydrogen bonding between polar heads in lipid bilayers.

The results reported here were obtained by using the the extrapolation method of Ferrenberg and Swendsen [22]. The nature of the phase transitions was firmly established by means of the finite-size-scaling method of Lee and Kosterlitz [18, 23].

From the point of view of hydrogen bonding in lipid bilayers, we have only described part of the behavior of the system at the main phase transition. For first-order phase transitions, we identify the low temperature fully bonded phase with the dehydrated or AS phase, which is therefore characterized by mostly bonding energy and small overall degeneracy. By contrast, the high temperature phase which is composed of mostly unbonding states and therefore represents a hydrated HS or HF phase, is characterized by a higher degeneracy and a small energy difference between lipid-lipid and lipid-water hydrogen bonds. What is missing in the model is a detailed analysis of the chain melting phase transition which accompanies change in the hydrogen bonding network. We intend to generalize the model to include these effects by using the Pink multistate lattice model [34] to describe the chain degrees of freedom for two chains at each lattice site. Nonhydrogen bonding interactions between polar heads and differences in free energy between the AS and HS phases will be introduced phenomenologically via additional energy and local entropy terms. Computer simulations of the same type as used in this paper will be applied to the full model so as to determine the phase behavior. Dynamics and metastability will also be examined in the spirit of the work done on quenching of Ising models.

We also plan to extend the model of Sec. II in order to apply it to the following problems:

(i) Binary mixtures of PE lipids and PC lipids which have only two acceptors and no donors.

(ii) Ternary mixtures of PE lipids, PC lipids, and diglycerides (DG) which do not hydrogen bond. This system should act in an analogous manner to a mixture of immiscible fluids containing surfactants with the PC lipids taking the part of surfactants.

(iii) Extension of the model of Sec. II to three dimensions. This should be a "toy" model for hydrogen bonding in water.

ACKNOWLEDGMENTS

This work was supported by the FCAR du Quebec under a center and team grant and by the NSERC of Canada under an operating grant. One of us (M.J.Z.) wishes to thank David Pink for many fruitful discussions on the modeling hydrogen bonding in lipid systems. J.T. acknowledges support from the Donors of The Petroleum Research Fund administered by the American Chemical Society.

* On sabbatical leave from Kalamazoo College, Kalamazoo, MI 49006.

[1] J.R. Silvius, P.M. Brown, and T.J. O'Leary, Biochemistry **25**, 4249 (1986).
[2] L.J. Lis, M. McAlister, N. Fuller, R.P. Rand, and V.A. Parsegian, Biophys. J. **37**, 657 (1982).
[3] J. Boggs, Can. J. Biochem. **52**, 3425 (1980).
[4] H. Hauser, I. Pascher, R.H. Pearson, and S. Sundell, Biochim. Biophys. Acta **650**, 21 (1981).
[5] P.B. Hitchcock, R. Mason, K.M. Thomas, and G. Shipley, Proc. Natl. Acad. Sci. U.S.A. **938**, 3036 (1974).
[6] J.M. Seddon, K. Harlos, and D.Marsh, J. Membr. Biol. **258**, 3850 (1983).
[7] J.M. Seddon, G. Cevc, and D.Marsh, Biochemistry **22**, 1280 (1983).
[8] H. Chang and R.M. Epand, Biochim. Biophys. Acta **728**, 319 (1983).
[9] H.H. Mantsch, S.C. Hsi, K.W. Butler, and D. Cameron, Biochim. Biophys. Acta **728**, 325 (1983).
[10] D.A. Wilkinson and J.F. Nagle, Biochemistry **23**, 1538 (1984).
[11] J.R. Silvius, Chem. Phys. Lipids **57**, 241 (1991).
[12] J.F. Nagle, J. Membr. Biol. **27**, 233 (1976).
[13] H. Eibl and J. P. Wooley, Biophys. Chem. **10**, 261 (1979).
[14] D.A. Pink, L. MacDonald, and B. Quinn, Chem. Phys. Lipids **47**, 83 (1988).
[15] L. MacDonald and D.A. Pink, Phys. Rev. B **37**, 3552 (1988).
[16] A. N. Berker, S. Ostlund, and F. A. Putnam, Phys. Rev. B **17**, 3650 (1978).
[17] A. Coniglio, H. E. Stanley, and W. Klein, Phys. Rev. B **25**, 6805 (1982).
[18] J. Lee and J.M. Kosterlitz, Phys. Rev. Lett. **65**, 137 (1990).
[19] A. Coniglio and W. Klein, J. Phys. A **13**, 2775 (1980).
[20] O.G. Mouritsen, in *Molecular Description of Biological Membrane Components by Computer aided Analysis*, edited by R Brasseur (CRC, Boca Raton, FL, 1990), Vol. 1, pp. 3–83.
[21] S.S. Challa, D.P. Landau, and K. Binder, Phys. Rev. B **34**, 1841 (1986).
[22] A.M. Ferrenberg and R.H. Swendsen, Phys. Rev. Lett. **61**, 2635 (1988).
[23] J. Lee and J.M. Kosterlitz, Phys. Rev. B **43**, 3265 (1991).
[24] D. Stauffer and H.F. Eicke, Physica A **182**, 29 (1992).
[25] D. Stauffer, *Introduction to Percolation Theory* (Taylor and Francis, London, 1984).
[26] J. Chalupa, P.L. Leath, and G.R. Reich, J. Phys. C **12**, L31 (1981); P.M. Kogut and I. Riess, Phys. Status Solidi B **69**, K15 (1975).
[27] Joan Adler, Physica A **171**, 453 (1991).
[28] J. Adler and A. Aharony, J. Phys. A **21**, 1387 (1988).
[29] J. Adler and D. Stauffer, J. Phys. A **23**, L1119 (1990).
[30] J. Adler and D. Stauffer, Physica A **175**, 222 (1991).
[31] J. Kertesz, Physica A **161**, 58 (1989).
[32] E.T. Gawlinski and H.E. Stanley, J. Phys. A **14**, L291 (1981).
[33] R. Lamanna and S. Cannistraro, Phys. Rev. A **46**, 7367 (1992).
[34] D.A. Pink, T.J. Green, and D. Chapman, Biochemistry **19**, 349 (1980).